Delft University of Technology

Vibration transfer from underground train to multi-story building

Modelling and validation with in-situ test data

Wang, Li; Gao, Xin; Zhao, Caiyou; Wang, Ping; Li, Zili

Important note
To cite this publication, please use the final published version (if applicable).
Please check the document version above.

Research Paper

Vibration transfer from underground train to multi-story building: Modelling and validation with in-situ test data

Li Wang [a], Xin Gao [b], Caiyou Zhao [b,*], Ping Wang [b], Zili Li [a,*]

[a] *Section of Railway Engineering, Delft University of Technology, Stevinweg 1, 2628CN Delft, The Netherlands*
[b] *Key Laboratory of High-speed Railway Engineering (Southwest Jiaotong University), Ministry of Education, Chengdu 610031, China*

Abstract

Excessive underground train-induced vibration becomes a serious environmental problem in cities. To investigate the vibration transfer from an underground train to a building nearby, an explicit-integration time-domain, three-dimensional finite element model is developed. The underground train, track, tunnel, soil layers and a typical multi-story building nearby are all fully coupled in this model. The complex geometries involving the track components and the building are all modelled in detail, which makes the simulation of vibration transfer more realistic from the underground train to the building. The model is validated with in-situ tests data and good agreements have been achieved between the numerical results and the experimental results both in time domain and frequency domain. The proposed model is applied to investigate the vibration transfer along the floors in the building and the influences of the soil stiffness on the vibration characteristics of the track-tunnel-soil-building system. It is found that the building vibration induced by an underground train is dominant at the frequency determined by the P2 resonance and influenced by the vibration modes of the building. The vertical vibration in the building decreases in a fluctuant pattern from the foundation to the top floor due to loss of high frequency contents and local modes. The vibration levels in different rooms at a same floor can be different due to the different local stiffness. A room with larger space thus smaller local stiffness usually has higher vibration level. Softer soil layers make the tunnel lining and the building have more low frequency vibration. The influence of the soil stiffness on the amplification scale along the floors of the building is found to be nonlinear and frequency-dependent, which needs to be further investigated.

Keywords: Railway vibration; Underground train; Multi-story building vibration; Finite element model; Dynamic interaction

1 Introduction

In many modern cities with dense population, residential buildings have to be very close to the underground railway lines or even be built directly on metro depots so as to save land resource. However, when providing convenient transportation service, the underground trains can also cause undesirable vibration to the adjacent inhabitants. The vibration is primarily generated at the wheel-rail interfaces and then propagates via the track and tunnel into the surrounding soil layers (Thompson et al., 2019). It becomes a problem when the vibration arrives at the building nearby to make the floors and walls shake (Connolly et al., 2016).

Many measurements have been conducted to acquire the vibration levels from the train to the building nearby. Wei et al. (2011) carried out a field test on the vibration in a 6-story building close to an underground train station in Shanghai, China. They found that the maximum vertical acceleration generally decreased with the increase of the floor number (height). Ma et al. (2011a) performed an in-situ test in a physics laboratory of a university in Beijing, China. In their measurements, the underground train-induced vibration and the vibration induced by the traffic

---

on road are comparable. Sanayei et al. (2013) measured the underground train-induced vibration inside buildings and at an open field in Boston, the U. S. A. They concluded that the vertical vibration is usually greater than the horizontal components inside buildings, and there is no consistent trend in differences between the vibration at an open field and that inside a building. Ma et al. (2011b) measured the underground train-induced vibration at a historic building in Chengdu, China. It was found that the vibration in building increases fast when the train speed goes above 58 km/h. To make full use of the land area, over-track building in metro depot becomes more and more popular. Cao et al. (2018) measured the vibration in a 7-story residential building constructed in an elevated metro depot in Nanjing, China. They found that the vibration levels at the first two floors are much higher than those at the other floors. Zou et al. (2015) performed field measurements on the vibration on ground and inside a 3-story building in a metro depot at Guangzhou, China. It was found that the vertical vibration inside the building is significantly greater than the horizontal vibration on the straight track. While at the throat area near the curve track, the horizontal vibration is remarkably larger than the vertical vibration. Liang et al. (2023) measured the vibration in a multi-story building in a metro depot with a 3-story platform. It was found that the underground train-induced vibration is more attenuated from the ground to the platform than from the platform to the building floors. Besides the measurements about the underground trains, the experiments on the vibration induced by the traditional over-ground trains are also of reference value. Xia et al. (2009) conducted a field experiment to study the train-induced vibration in a 6-story masonry building in a suburb of Shijiazhuang, China. The train speed varied from 40 to 115 km/h for passenger trains and from 26 to 57 km/h for freight trains. They found that the building vibration generally increases as the train speed increases. Although all of the experimental results above are only responsible for the specific cases, these measurements provide important basic understandings about the underground train-induced vibration in a building.

To further estimate and predict the vibration level caused by an underground train and also to assess the effectiveness of a vibration mitigation measure, many analytical and numerical methods/models have been developed (Sheng, 2019). Trochides (1991) presented an analytical method from energy considerations based on approximate impedance formulae for the tunnel and the building. Comparisons between calculations and measurements showed the method acceptable for design purposes. Yang and Huang (2008) proposed a 2.5-dimensional (2.5D) finite/infinite element approach to analyze the wave propagation problems caused by the underground trains. It was found that the ground surface vibration can be greatly reduced when the tunnel is built on a stiffer soil. Zou et al. (2021) developed an analytical impedance model accounting for the wave transmission through the columns and load-bearing walls commonly found in the over-track buildings. Good agreements with the field tests prove this model an efficient and cost-effective tool for estimating floor vibration before construction. Coulier et al. (2014) employed a coupled finite element–boundary element methodology to analyze the interaction between a building and a railway tunnel. It was found that the vibration source-receiver interaction can be neglected only when their distance is sufficiently large compared with the soil wavelength. He et al. (2020) proposed a three dimensional (3D) analytical method to predict the vertical building vibration induced by underground trains. It was found that building vibrations are greatly influenced by the dynamic properties of a building and the building-ground interaction. Due to the complexity of the problem, hybrid methods are more common for the prediction of building vibration induced by an underground train. Lopes et al. (2014b) proposed a hybrid numerical approach containing a multi-body train model, a 2.5D track-tunnel-ground system and a 3D finite element (FE) modelling of building. Qu et al. (2021) put forward a hybrid methodology involving the vehicle-track dynamics (multi-body method), the wavenumber finite element theory (2.5D FEM) and the Green's function method (unit impulse excitation). Yang et al. (2019) presented a two-step prediction method in which the rail supporting forces are obtained in the first step through the spatial train-track coupled dynamic model and then applied in the second step as external loads into a FE track-tunnel-soil-building model to calculate the building vibration. S. Wang et al. (2022) proposed a two-step hybrid approach in which the fastening forces were first obtained in the 3D vehicle-track-foundation subsystem and then applied into the 2D track-tunnel-soil layers subsystem. Colaço et al. (2022) presented a hybrid methodology combining numerical/experimental results and post-processing techniques to assess the dynamic response of a structure.

In general, the analytical and numerical methods above successfully fulfilled their objectives, but there are still some drawbacks. The analytical methods have difficulties in considering the complex geometry of a residential building with irregular shapes. The 2.5D approach usually requires invariance or periodicity of the structure in the train's moving direction, and therefore a specific building is difficult to be embedded. A hybrid method usually involves multiple techniques, such as the multibody dynamics and the FE method, which may demand a higher level of expertise. Moreover, additional assumptions may be required to make the separate steps or sub-models compatible, potentially leading to inaccuracies in the simulation results. Additionally, many assumptions in the coupling process, such as a weak coupling between the building structure and the railway infrastructure, will limit the application of a hybrid method, especially in the cases where the buildings are too close to the railway lines that the added-building effect cannot be ignored (Sanitate & Talbot, 2023).

With the rapid development of computational power, the FE method becomes more applicable to the problem

(Ibrahim & Nabil, 2021; L. Wang et al., 2022). In the present work, an explicit FE method is employed. A fully coupled 3D train-track-tunnel-soil layers-building FE model is developed and validated with in-situ tests data. All the parts in this model are fully coupled without any additional coupling assumption. The complex geometries of the track structure and a typical multi-story residential building are considered in detail thus making the simulation of vibration transfer more realistic and accurate. The paper is organized as follows. In Section 2, the in-situ tests are introduced. Section 3 presents the modelling method in detail. In Section 4, the model is validated with the in-situ tests data in both time domain and frequency domain. In Section 5, the vibration at the source (train-track interaction in tunnel), along the transmission path (in soil layers) and at the receiver (in the building) are discussed, respectively. Finally, the main findings are presented.

2 In-situ tests

The in-situ tests were conducted at a typical multi-story building which is very close to an underground line in Chengdu, China. The distance from the building to the track center is only 17 m in horizontal direction, as illustrated in Fig. 1. The tunnel is in the soil layers with a depth of 23 m from the ground surface to the cross-section center of the tunnel.

The building is 92 m tall with 30 stories above the ground surface and about 20.5 m in depth with a 4-story basement. The building was just finished without residents inside. In our experimental campaign, the dynamic responses of the track structure, the tunnel, and the building were measured during the underground train passages. The rail surface roughness and the properties of the soil layers nearby were also measured.

2.1 Tests in tunnel

The tunnel at the test site is close to an underground train station where two underground lines meet each other. The tunnel cross-section is circular with an inner radius of 2.7 m and a wall thickness of 0.3 m. There is a twin tunnel at the same depth and the twin tunnel is farther from the building. The distance between the centers of the two tunnels is 15 m. The train passages in the twin tunnel were not measured because there was no situation when two trains met at the test site which can cause additive effect.

The track structure contains rails (CHN60), fasteners, track slabs and an adjusting layer over the concrete base, as shown in the zoom-in on the lower right corner of Fig. 1. The vertical accelerations at the rail, slab and tunnel were measured, as shown in Fig. 2.

The vertical rail acceleration was measured with an accelerometer attached at the rail foot bottom. Close to
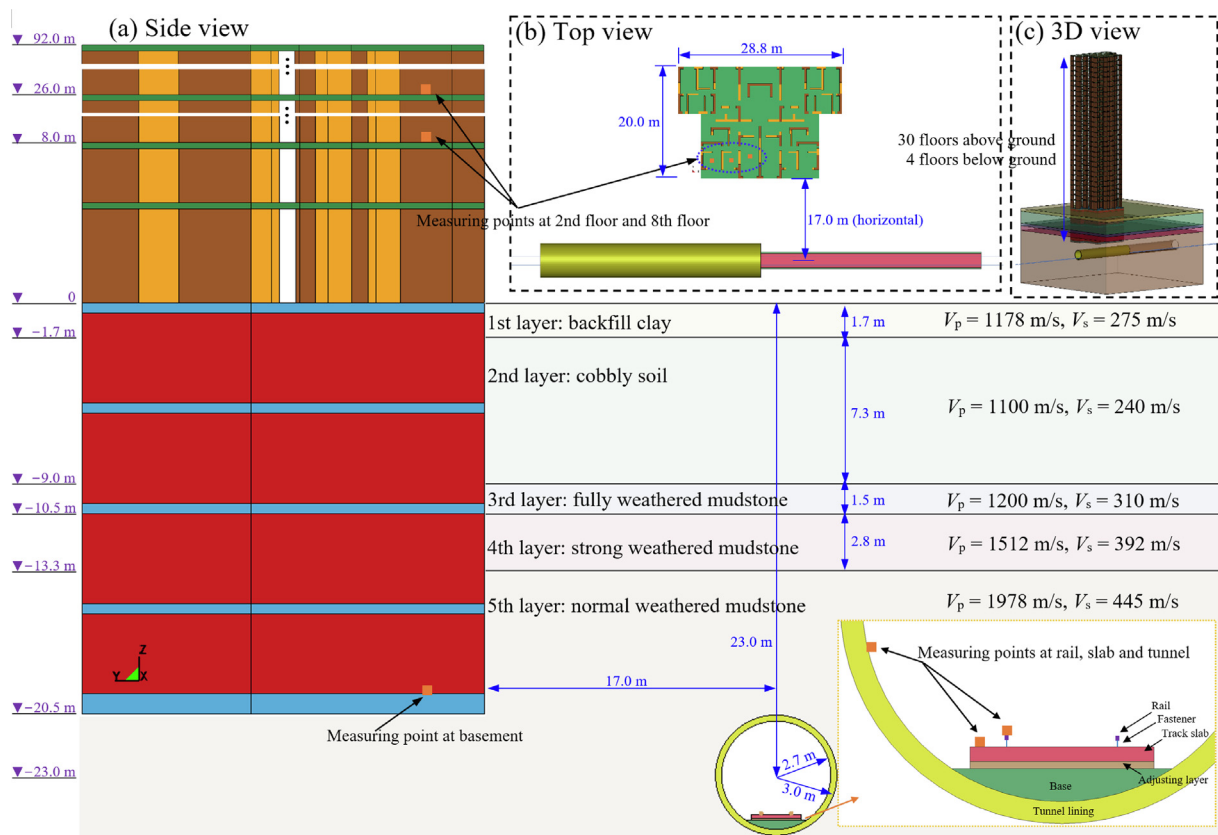

Fig. 1. Overview of the test site. (a) Side view, (b) top view, and (c) 3D view. (V_p – primary wave velocity, V_s – secondary wave velocity).

Fig. 2. Measurements in the tunnel.

the accelerometer at the rail, in the same track cross section, an accelerometer was attached on the track slab to measure the vertical vibration transferred to the slab. The accelerometer on the tunnel wall was about 1.25 m above from the rail top surface (Ministry of Ecology and Environment of the People's Republic of China, 2018). The sampling frequency for all the three accelerometers were 5120 Hz.

The rail surface roughness at the test site was measured in the wavelength range of 0.005–1.000 m, as shown in Fig. 3.

It can be seen in Fig. 3(b) that the roughness level exceeded the standard limit quite a lot in the wavelength range of 0.020–0.400 m. Thus, there could be many complains if no vibration mitigation measure was taken.

2.2 Tests in the building

Only the vertical vibrations at the −4th, 2nd and 8th floors were measured due to the availability, as shown in Fig. 1. The building is symmetrical, as shown in Fig. 4.

Above the ground, each floor of the building consists of 4 apartments. The two smaller apartments are closer to the tunnel and also symmetrical to each other along a plane perpendicular to the railway line. The measurements were conducted in the small apartment in the lower left corner in Fig. 4. The non-load-bearing walls (yellow in Fig. 4 (b)) make each apartment into several rooms. In the measured apartment on the 2nd floor, three accelerometers were installed at the centers of the three rooms, i.e., Room 1, Room 2 and Room 3, as illustrated in Fig. 4(b). The measurements on the 8th floor were done with the same configuration. The −4th floor is the deepest floor in the basement, where no non-load-bearing wall exists, and thus no separate rooms. Only one accelerometer was installed on the −4th floor, right under the position of the sensor in Room 1 on the 2nd floor. The positions of the accelerometers and the dimensions of the rooms are shown in Fig. 4. The sampling frequency was 2048 Hz.

The measurements in the building were not synchronous for different floors, and also not synchronous with the measurements in the tunnel. However, the train schedule was the same every day at the test site. At the same particular time slot of the consecutive measurement days, the passing train was almost the same train.

2.3 Stratification

The soil properties were obtained from a borehole between the building and the tunnel. There are five soil layers and the tunnel is in the 5th layer which is full of normal weathered mudstone. The depth, the density and the primary and secondary wave velocities of each soil layer are
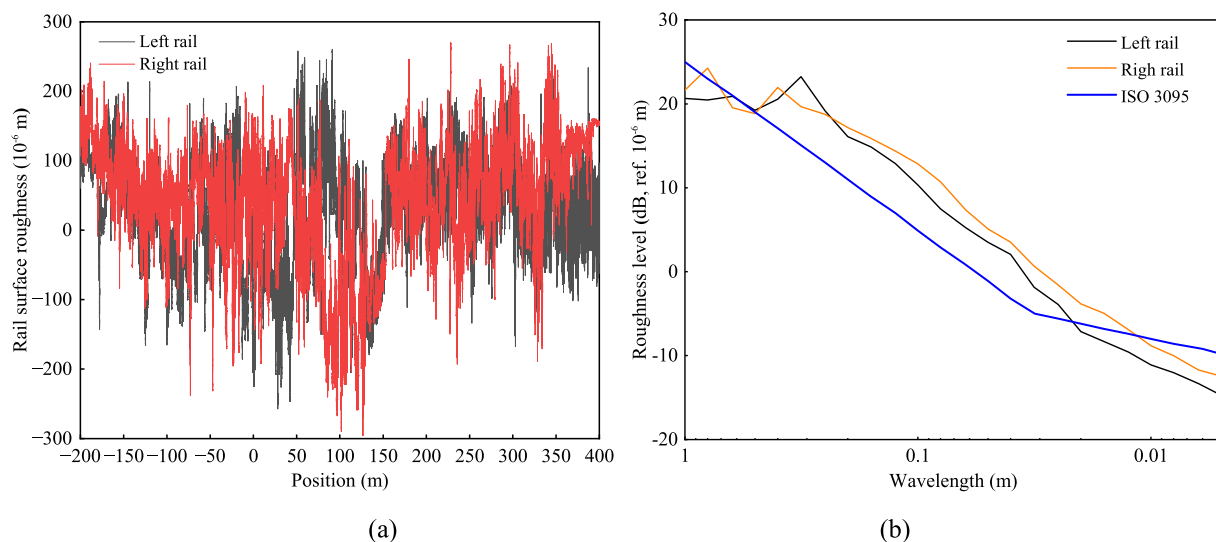

(a)

(b)

Fig. 3. Measured rail surface roughness at the test site. (a) Left and right rail surface roughness, and (b) roughness level (International Organization for Standardization, 2013).
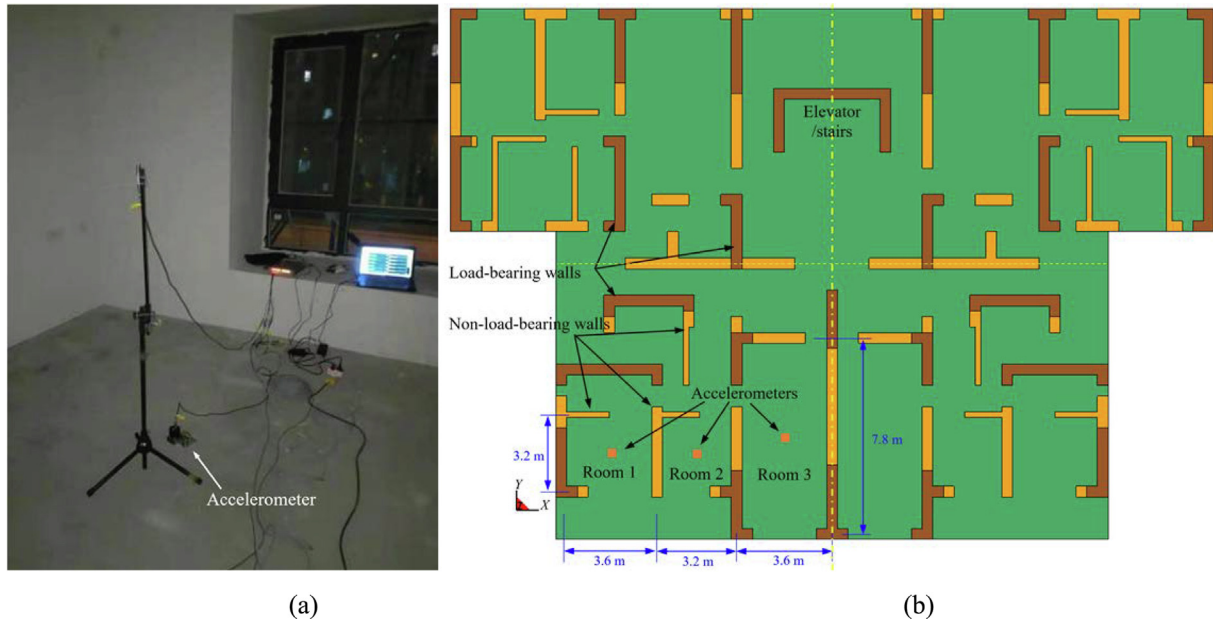
Fig. 4. Measurements in the building and the dimensions of the three rooms. (a) Measurements in the building, and (b) top view of the three rooms.

listed in Fig. 1. Worth mentioning is that, the borehole was carried out before the construction of the building. The construction could possibly influence the soil properties to some extent (L. Wang et al., 2022).

3 Modelling method

3.1 Modelling overview

An explicit-integration time-domain, 3D dynamic, fully coupled, train-track-tunnel-soil-building FE model is established. As shown in Fig. 5(a), the main part of the model is 98 m in length in the longitudinal direction (train's moving direction). The two rails of the track are extended at the two ends of the main part in order to properly consider the approaching and leaving of an underground train which is about 120 m long. At the approaching end and the leaving end, the rails are extended 200 and 400 m, respectively. The extended rails are with simplified supports thus limiting the overall model within a reasonable size to be computationally efficient. The depth of the model is up to 45 m below ground so as to cover the five soil layers in Fig. 1. The width of the model is 96 m. In the in-situ tests, only the train passages in the tunnel closer to the building were recorded. Therefore, only one tunnel is considered in this modelling. The effect of the twin tunnel is ignored.

3.2 Underground train modelling

The underground trains running at the test site were Chinese Type-B metro trains. There are 6 vehicles for each train. In the train modelling, as shown in Fig. 5(b), the carbody, two bogies and the secondary suspensions of each vehicle are together lumped into 8 equal mass points. The

4 wheelsets of each vehicle are lumped into 8 mass points accordingly. The primary suspensions are modelled as springs and dampers connecting the 8 pairs of mass points. The vehicle length L, bogie spacing L_b and axle spacing L_a are 19.6, 12.6 and 2.3 m, respectively. The mechanical parameters of the train are listed in Table 1 (Ma et al., 2021).

In the longitudinal direction (X-direction, i.e., train's moving direction, as shown in Fig. 5), all the mass points are coupled together traveling with the same longitudinal train speed, and there is no relative longitudinal movement between the mass points. In the lateral direction (Y-direction), the displacements of the mass points are fully constrained. In the vertical direction (Z-direction), there is no special constraint on the mass points.

3.3 Track structure and tunnel

The two rails are modelled with beam elements. The fasteners are modelled as springs and dampers. The other components, namely, the slab, adjusting layer, base and tunnel are all modelled with 8-node solid elements, as shown in Fig. 5(c). The adjusting layer is made up of self-compacting concrete. The mechanical parameters of the components in the tunnel are listed in Table 2 (L. Wang et al., 2022).

The classical Rayleigh damping method is adopted to consider the possible damping of the track components:

$$C = \alpha M + \beta K, \tag{1}$$

where α and β are the proportional constants of the mass matrix M and stiffness matrix K, respectively.

The values of α and β, as listed in italic in Table 2, are determined through trial simulations in the validation pro-
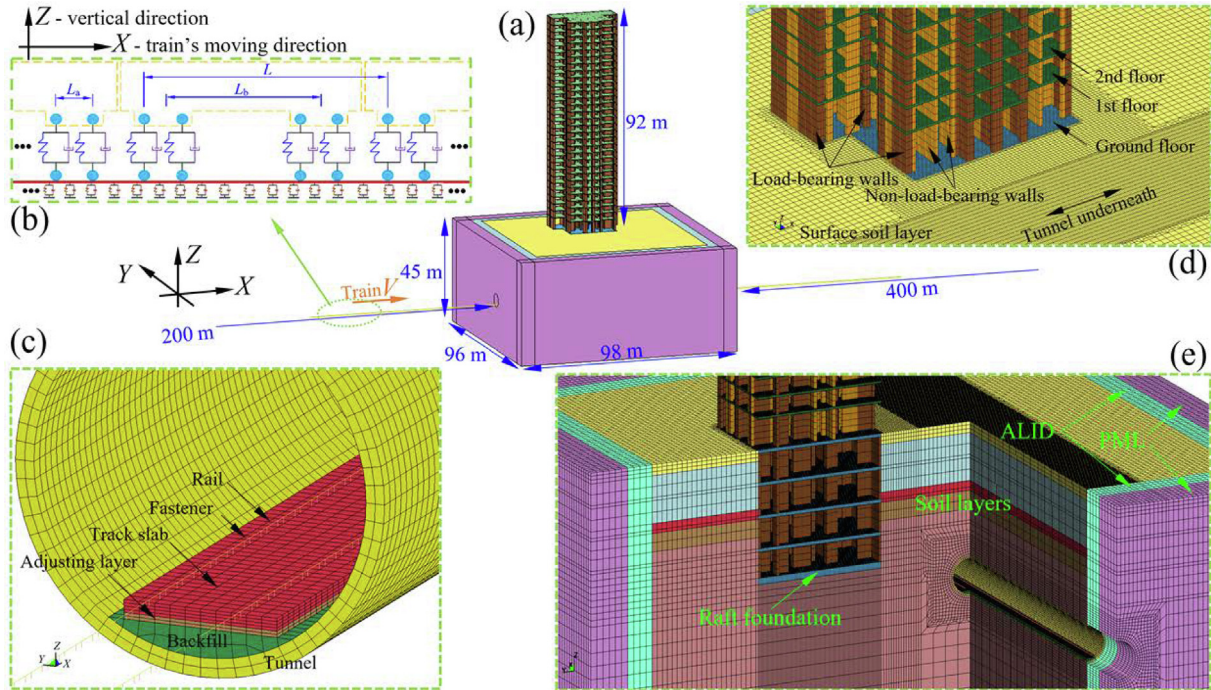
Fig. 5. Fully coupled 3D train-track-piles-soil-building FE model. (a) Dimensions, (b) train model, (c) walls and floors in building and local mesh, (d) track structure and tunnel, and (e) perfectly-matched layer (PML), absorbing layers by increasing damping (ALID) and mesh of soil layers (cross sections).

Table 1
Parameters of vehicle.

Vehicle component	Mass (kg)	Stiffness (N/m)	Damping (N·s/m)
Car body	49 700	–	–
Bogie	3740	–	–
Wheelset	1530	–	–
Primary suspension	–	1.3×10^6	1.3×10^4

cess. The same method is also applied to the soil layers and the building (see Section 3.4 below).

The fasteners at the test site are the Chinese subway fasteners. The mechanical properties of the fasteners are determined using trial and error method until decent agreements are achieved between the simulation results and the measured dynamic responses at the rail, slab and the tunnel wall in both time domain and frequency domain. For the fasteners at the approaching and leaving parts, the parameters are obtained also by trial simulations to ensure that their rail deflections are at the same level as that of the main part to avoid unphysical disturbances at the transi-

tions between the main part and the extended parts (L. Wang et al., 2022). The parameters of the fasteners are listed in Table 3.

The wheel-rail contact is defined as the wheel mass points moving along the rails. The vertical contact force F is

$$F = K_H \cdot (Z_W - Z_R - \delta), \tag{2}$$

where K_H is the contact stiffness, Z_W is the displacement of wheel, Z_R is the displacement of rail, and δ is the input rail roughness (see Fig. 3). A linear contact stiffness of 1.32×10^9 N/m is assumed (Li et al., 2020; L. Wang et al., 2022), while no tensile force is generated when the wheel loses contact with the rail. Both the left and right rail roughness are considered.

3.4 Soil layers and building

The building and the soil layers are modelled with 8-node solid elements. The dimensions of the elements are

Table 2
Parameters of the track and substructures.

Track component	Elastic modulus (MPa)	Poisson's ratio	Density (kg/m³)	Rayleigh damping	
				α (s⁻¹)	β (s)
Rail	2.06×10^5	0.3	7800	–	–
Track slab	3.45×10^4	0.2	2350	0	0.0001
Adjusting layer	2.0×10^3	0.2	1900	0	0.0005
Base	3.0×10^4	0.2	2200	0	0.0002
Tunnel	3.4×10^4	0.2	2400	0	0.0001

Table 3
Parameters of fasteners.

Position	Stiffness(N/m)	Damping(N·s/m)
At the main part	160×10^6	40 000
At the approaching and leaving parts	100×10^6	40 000

between 0.2 and 2.2 m. The geometries of the walls, floors, ceilings and the raft foundation are considered accurately where necessary. The parameters of the soil layers and the building are listed in Table 4.

3.5 Boundary considerations and computational implementation

To make the FE model within a reasonable size, the soil layers need to be truncated. At the boundaries, an approach of absorbing layers by increasing damping (ALID) and the perfectly-matched layers (PML) are used to first damp and then absorb the outward vibration waves, as shown in Fig. 5(e). In this way, the wave reflection is limited to the least extent as possible.

The simulations are performed using the commercial software ANSYS/LS-DYNA. In total, there are 1 689 636 elements and 2 151 051 nodes. The time step is fixed at 1.05×10^{-5} s. The calculation time for each case takes about 63 h by a workstation with a 12-core 2.69 GHz processor.

4 Model validation

In this section, the proposed FE model is validated against the in-situ tests data in both time domain and frequency domain. With the parameters in the four tables above, the measured responses at the measuring points in the tunnel and in the building should be reproduced to a large extent by the proposed numerical model.

4.1 Validation in time-domain

The maximum acceleration value peak particle acceleration (PPA) and the weighted vibration severity $KB_F(t)$ are

two usual indicators to access the effect of vibration (Deutsches Institut für Normung, 1999; Kouroussis et al., 2011; Li et al., 2020; Thompson et al., 2019; L. Wang et al., 2022). PPA is defined as the maximum absolute amplitude of the acceleration signal in time domain:

$$PPA = \max |a(t)|, \tag{3}$$

where t is the recording time. Weighted vibration severity $KB_F(t)$ is the time-averaged signal (running root mean square) of $KB(t)$, defined as

$$KB_F(t) = \sqrt{\frac{1}{\tau} \int_0^t KB^2(\xi)e^{-(t-\xi)/\tau}d\xi}, \tag{4}$$

where the time constant τ is 0.125 s, and the weighted acceleration signal $KB(t)$ is obtained by passing the original acceleration signal through the high-pass filter:

$$|H_{KB}(f)| = \frac{1}{\sqrt{1 + (f_0/f)^2}}, \tag{5}$$

where f is frequency and the cut-off frequency f_0 is 5.6 Hz. The maximum absolute amplitude $KB_F(t)$ is denoted as KB_{Fmax}:

$$KB_{Fmax} = \max |KB_F(t)|. \tag{6}$$

The PPA and the KB_{Fmax} of the vibration at each measurement location from the rail to the building are presented in Fig. 6 for the 10 train passages at around 70 km/h.

In Fig. 6, each black circle is the maximum value, i.e. maximum $a(t)$ in Fig. 6(a) or maximum $KB_F(t)$ in Fig. 6(b), during each complete underground train's passing-by. It can be seen from Fig. 6 that, for the two indicators, the change trends are quite similar. The vibration acceleration decreases dramatically from the rail to the building. At the rail, the vertical vibration acceleration can be up to 200 m/s², which is probably because of the roughness at the wheel-rail contact. At the track slab, the maximum vibration acceleration decreases to approximately 5 m/s² with the damping effect from the fasteners. The vibration acceleration at the tunnel lining is further reduced but not much as there is no specific measure for vibration reduction between the track and the tunnel. The vibration acceleration is significantly reduced when it arrives at the

Table 4
Parameters of soil layers and the building.

Component		Elastic modulus (MPa)	Poisson's ratio	Density (kg/m³)	Rayleigh damping	
					α (s^{-1})	β (s)
Soil layers	1st layer	422	0.47	1900	0.1	0.04
	2nd layer	356	0.47	2100	0.1	0.04
	3rd layer	577	0.47	2050	0.1	0.04
	4th layer	994	0.47	2210	0.1	0.04
	5th layer	1365	0.47	2300	0.1	0.06
Building	Floors	28 000	0.2	2000	0	0.01
	Load-bearing walls	30 000	0.2	2200	0	0
	Non-load-bearing walls	24 000	0.2	1800	0	0
	Foundation	32 000	0.2	2400	0	0.01

building, ranging between about 0.02 and 0.1 m/s², owing to the damping effect of the soil layers. In the building, the amplitude of the measured vibration acceleration at each measuring point varies a lot, but in general, the vibration acceleration decreases slowly from the −4th floor to the 8th floor. At the 2nd floor, the vibration amplitudes are different in the separate rooms. The vibration acceleration in average in Room 3 is the highest while that in Room 2 is lowest of the three rooms. Similar difference can be found at the 8th floor. Further discussion about the vibration in the building will be presented in Section 5. With the proposed model, the attenuation of PPA and of KB_{Fmax} from the rail to the 8th floor of the building are successfully simulated, as shown with the red solid lines in Fig. 6.

Figure 7 presents in detail the time-histories of vertical accelerations at various locations during a typical underground train's passing-by with the train speed of about 70 km/h. The measurements are overlaid with the simulations thus for a fully comparison.

It can be seen from Fig. 7 that, in general and for all the measurement locations, the numerical results correspond all quite well to the experimental results, both in maximum magnitude and contour-shape. At the rail and the slab, the

responses to the passing of each wheelset are distinguishable, as shown in Fig. 7(a) and (b). The responses cannot be distinguished between the wheel passages at the tunnel wall and in the building.

4.2 Validation in frequency-domain

The vibration acceleration level (VAL) is widely used to evaluate the vibration level at a specific location in frequency domain (Liang et al., 2022; Ma et al., 2022; Thompson et al. 2019). The VAL is defined as:

$$\text{VAL}(f_i) = 20 \lg \frac{a(f_i)}{a_0}, \tag{7}$$

where $a(f_i)$ is the root mean square (RMS) of the acceleration at the 1/3 octave band center frequency f_i. a_0 is the reference acceleration, and $a_0 = 10^{-6}$ m/s².

Figure 8 presents the vertical VALs at the rail, slab, tunnel wall and the measuring points in the building.

It can be seen from Fig. 8(a) that, the vibrations at the rail, slab and tunnel wall are distributed in quite a wide frequency range. There is a common peak at around 80 Hz. This peak frequency is mainly determined by the fastener stiffness and the wheel mass, i.e. P2 resonance, which can be confirmed by parameter study. There is also high frequency content above 200 Hz, which is mainly attributed to the rail and wheel surface roughness (Liang et al., 2022; Ma et al., 2022; Qu et al., 2023; Xu et al., 2016). From Fig. 8(b), (c), and (d), it can be seen that the frequency contents of the responses at all the measuring points in the building are quite similar. They have mainly one common peak of around 80 Hz. From the tunnel to the building, much high frequency contents have been damped by the soil layers. From Fig. 8, it can be seen that, in general, the frequency contents in the experimental results are well reproduced in the numerical results, especially in the frequency range from 5 to 200 Hz.

With the comparisons in time domain and frequency domain, it can be safely concluded that the proposed model is able to simulate the vibration transfer from the underground train to the building.

5 Discussions

In this section, parameter study with various fastener properties and soil properties will be conducted in order to investigate how the vibration transfer is influenced at the vibration source (in tunnel) and at the transmission path (in soil). Also, the vibration levels at various floors in the building are calculated to discuss how the vibration travels in the building.

5.1 Vibration in the building

The building, as a vibration receiver, will vibrate accordingly when the incident waves arrive. To evaluate the effect of vibration on humans, the weighted vertical vibration
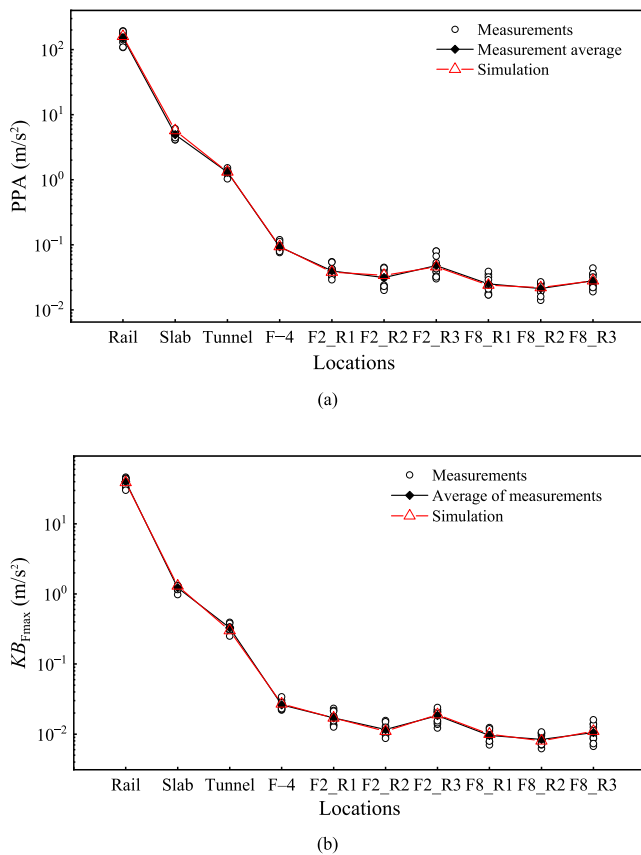

Fig. 6. Vibration transfers from rail to the building. (a) PPA, and (b) KB_{Fmax}. (F-4: the − 4th floor in the basement; F2_R1: Room 1 on the 2nd floor; F2_R2: Room 2 on the 2nd floor; F2_R3: Room 3 on the 2nd floor; F8_R1: Room 1 on the 8th floor; F8_R2: Room 2 on the 8th floor; F8_R3: Room 3 on the 8th floor).
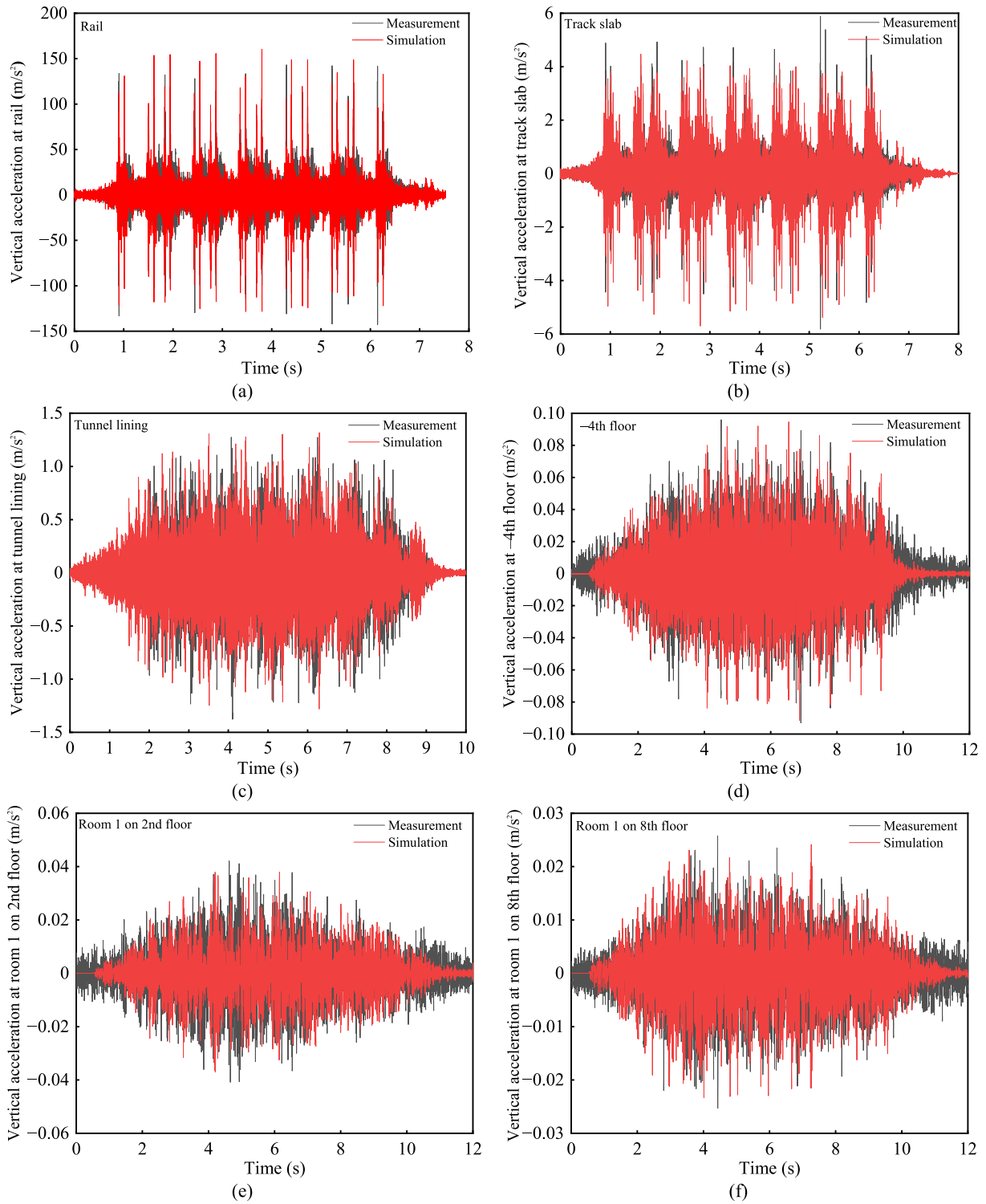
Fig. 7. Measured and simulated histories of vertical accelerations at various locations during the passage of a typical underground train at the speed of 72 km/h. (a) Rail, (b) track slab, (c) tunnel lining, (d) the –4th floor, (e) Room 1 on the 2nd floor, and (f) Room 1 on the 8th floor.

level (VL) at each room of each floor is calculated (International Organization for Standardization, 1997; Liang et al.,2022):

$$VL = 10\lg\left(\sum_{i=1}^{n} 10^{\frac{VAL(f_i)+W(f_i)}{10}}\right),\qquad(8)$$

where $W(f_i)$ is the weighting factor at each center frequency f_i of the 1/3 octave band. Frequency range of 0.1–400 Hz is considered (International Organization for Standardization, 1997), thus here n is 37.

Figure 9 shows the simulated weighted vertical vibration levels at various observing points along the floors.
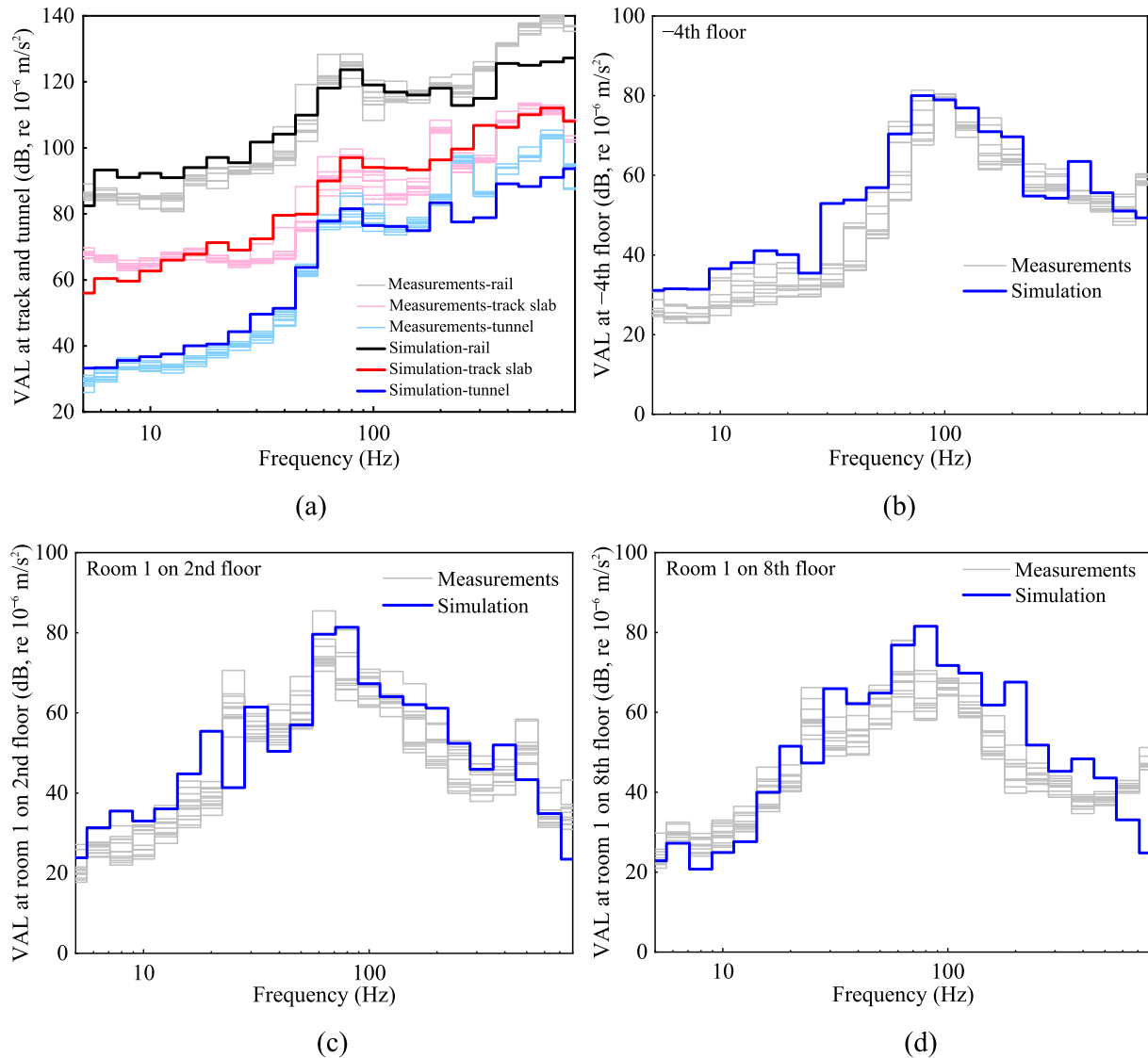
Fig. 8. Measured and simulated VAL at each measuring point. (a) Rail, track slab and tunnel lining, (b) the −4th floor, (c) Room 1 on the 2nd floor, and (d) Room 1 on the 8th floor.

It can be seen in Fig. 9 that the vertical vibration level decreases in a fluctuant pattern as the floor number increases. The vertical vibration level decreases generally along the floors and locally amplifies at some floors as indicated with the arrows in Fig. 9(b). The vertical vibration level deceases generally because there is structural damping in the building. The vertical vibration level amplifies at some floors may be because of some local modes (Ju, 2007; Mendoza et al., 2020), which needs to be further investigated.

The vibration level at the −4th floor is much lower than those at the other floors in the basement because the raft foundation makes the −4th floor much thicker thus stiffer than the other floors. In other words, the local stiffness influences a lot the vibration level in a building. The difference in the vertical vibration level in the different rooms at a same floor can also be attributed to the variance in local stiffness. As shown in Fig. 9(a), Room 2 is smaller than the

other two rooms while Room 3 is the largest room in the apartment. Thus, the local stiffness of Room 2 is the largest while the local stiffness of the Room 3 is the smallest. Therefore, the vibration level in Room 3 is always the highest while the vibration level in Room 2 is always the lowest of the three rooms. To further confirm this, it can be seen from the green line in Fig. 9(b) that, the vertical vibration level at a corner in Room 3 is always the smallest because the local stiffness at a corner is larger than that at the middle of a room. In Fig. 9(b), as specified in the Chinese standard (State Environmental Protection State Environmental Protection, 1988), 70 dB and 67 dB are the allowable maximum vertical vibration levels at day and night, respectively. It is obvious that the vibration levels are too high at many floors, especially at low floors. Vibration mitigation measures should be investigated and adopted.

To further investigate the vibration amplification or reduction along the height of the building, the amplifica-

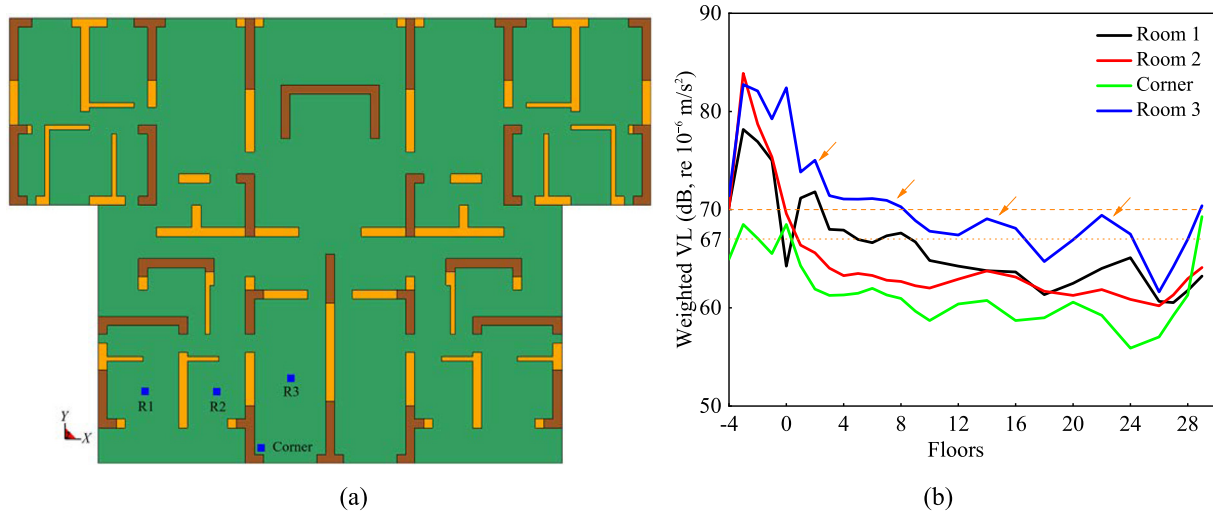(a)   (b)

Fig. 9. Simulated weighted vertical vibration levels at various observing locations along floors. (a) Observing points, and (b) weighted vertical vibration levels.

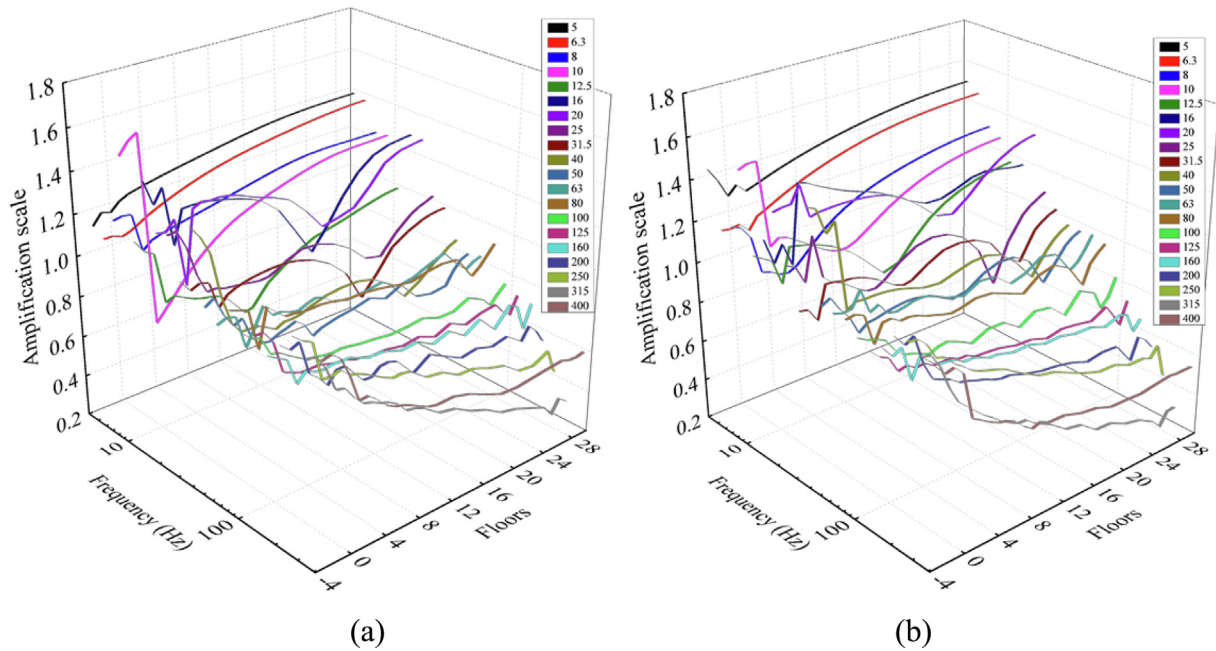(a)   (b)

Fig. 10. Amplification scale along the floors (Legends list the center frequencies of 1/3 octave bands). (a) At the center of the floor on which Room 1 is, and (b) at the corner of Room 3.

tion scale $S(f_i)$ at each center frequency f_i of a 1/3 octave band is defined and calculated as follows:

$$S(f_i) = \mathrm{VAL}_{j\mathrm{th}}(f_i)/\mathrm{VAL}_{-4\mathrm{th}}(f_i), \tag{9}$$

where $\mathrm{VAL}_{j\mathrm{th}}(f_i)$ is the vibration acceleration level at the jth floor and $\mathrm{VAL}_{-4\mathrm{th}}(f_i)$ is the vibration acceleration level at the -4th floor, i.e. the building foundation.

Figure 10 shows the amplification scale along the height of the building at the floor center of the floor where Room 1 is located, and at the corner of Room 3.

In Fig. 10(a), it can be seen that the amplification scale varies a lot at different octave bands. In general, at low fre-

quency bands, such as at the 5, 6.3 and 8 Hz, the vibration amplifies along the height of the building except in the basement. While at high frequency bands, such as above 100 Hz, the vibration mainly decreases along the floors of the building.

In Figs. 9 and 10, the amplification or reduction of the vibration at the floor center or the corner of a room along the height of the building may be attributed to the resonance of the building. To find more details of the resonance of the building, the vibration modes of the building are obtained by modal analysis using FE method. Five typical vibration modes are as shown for example in Fig. 11.
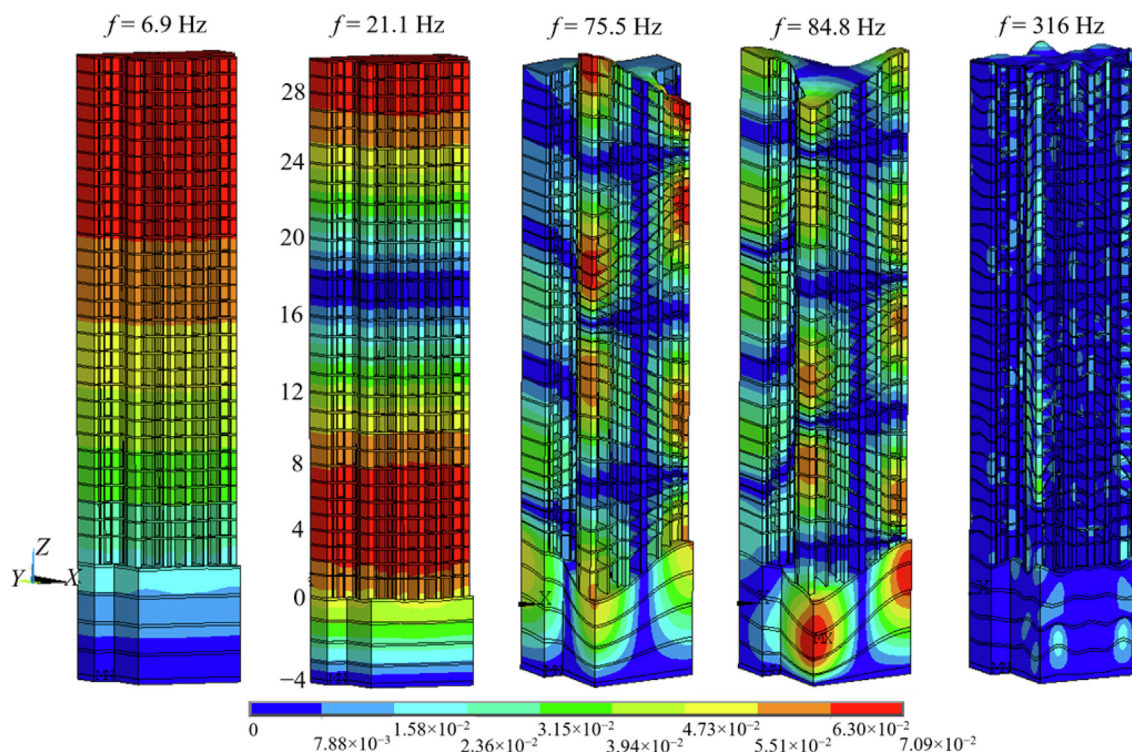
Fig. 11. Typical vertical vibration modes of the building.

In the modal analysis, the building is constrained in the lateral direction, thus the analysis focuses on the vertical vibration because the vertical vibration is much more dominant in the measurements. It can be seen in Fig. 11 that, at the frequency 6.9 Hz, the vibration amplitude increases along the floors. Thus, the vibration amplification scale increases along the floors, which is in line with the trends at frequency 6.3 Hz in Fig. 10 (see the red lines). At 21.1 Hz, longitudinal vibration can be seen along the floors. At some floors, such as the 4th–7th floors, the vertical vibration is amplified, while at the other floors, such as the 17th and 18th floors, the vertical vibration is reduced. This is also to some extent in line with the trends at 20 and 25 Hz in Fig. 10 (see the purple and dark red lines). At higher frequencies 75.5 and 84.8 Hz, more complex local vibration can be observed. The vertical vibration is not only varied along the floors but also different in different rooms at a same floor. At a much higher frequency 315.8 Hz, the resonance can be very localized at some specific locations of the building.

From the previous analysis of the measurements and simulations of the building responses, it is shown in Fig. 8 that, the major frequency content of the responses at various floors of the building is around 80 Hz. But from the modal analysis of the building, no vertical vibration mode can be found at about 80 Hz which can make vertical vibration of the −4th floor, 2nd floor and 8th floor amplified simultaneously. Therefore, the building vibration in the present case is mainly induced by the passing underground train rather than the building resonances. How-

ever, since some consistencies have been found between the amplification scales in Fig. 10 and the building resonances in Fig. 11, it can be deduced that the building resonance also contributes to the train-induced building vibration. In summary, the vertical vibration of the building is dominant at the frequency determined by the P2 resonance and influenced by the vibration modes of the building.

5.2 Influence of soil stiffness

The soil layers play a key role influencing the vibration transfer from the underground train to the building (Lopes et al., 2014a; Yang & Huang, 2008), and this can be seen from Fig. 8(a) to Fig. 8(b) where it shows that large part of the high frequency contents is damped by the soil layers. In this section, three additional cases with various soil stiffness values are considered in order to investigate the influence of soil layers on the vibration transfer.

In Fig. 1, it can be seen that the first two soil layers are relatively soft compared with the following three soil layers which are all weathered mudstone. With a preliminary study, it is found that, compared with the lower three layers, the first two soil layers have much less influences on the building responses. It may be because of the particular soil geometry configuration in this location (see the thickness of each soil layer and the positions of building and the tunnel in Fig. 1). Thus, to simply the problem, the 3rd, 4th and the 5th soil layers are treated together as one layer in this parameter study. The focus is on this combined layer in

Table 5
Cases of the combined soil layer.

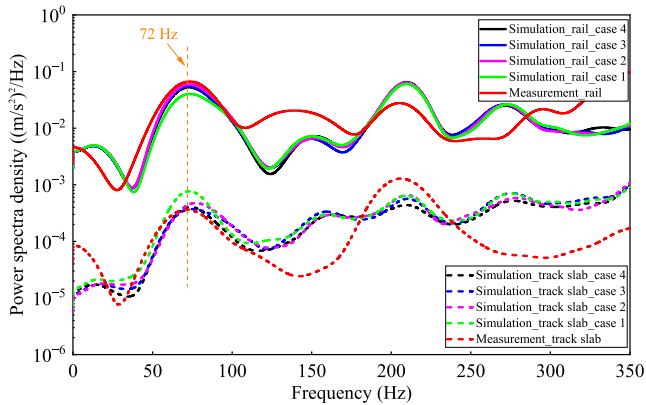| Case No.	Elastic modulus (MPa)
1	200
2	400
3	800
4	1365

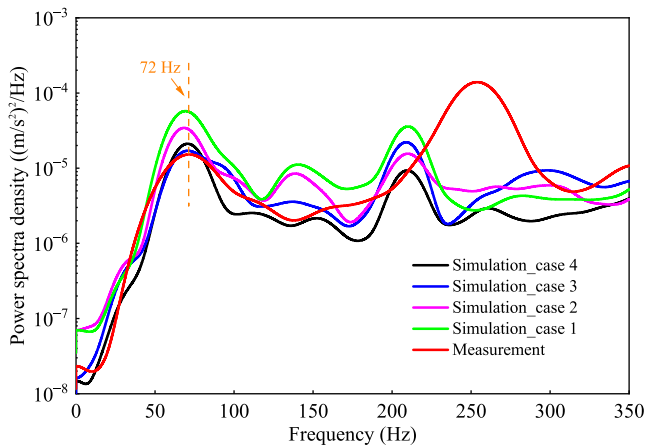Fig. 12. Influences of soil stiffness on the responses of rail and track slab.

Fig. 13. Influences of soil stiffness on the responses of tunnel lining.
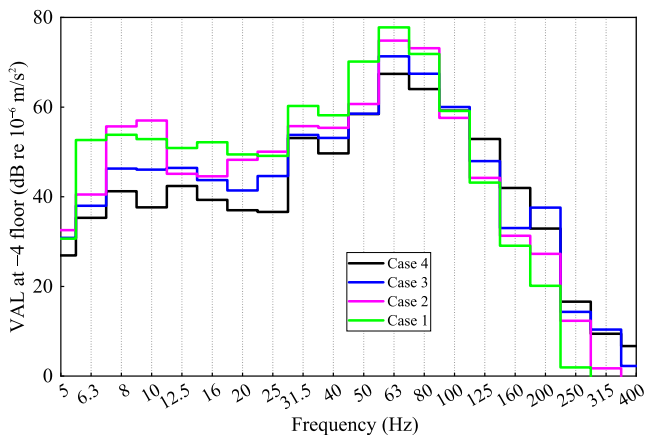

Fig. 14. Influence of soil stiffness on the response at the −4th floor.

which it contains the whole tunnel, the building foundation and the main part of the building basement. The cases considered for the soil stiffness of the combined soil layer are listed in Table 5. The properties of the first two soil layers and the other parameters are kept unchanged as listed in Tables 1–4.

The simulation results are shown in Figs. 12–14.

It can be seen from Fig. 12 that, the influence of soil stiffness on the rail dynamic response can be generally ignored, as shown with the solid lines. The soil stiffness has also very limit influence on the dynamic response of the track slab, as shown with the dash lines.

However, the dynamic response of the tunnel wall is noticeably changing when the soil stiffness is varying from 1365 to 200 MPa, as shown in Fig. 13.

It can be seen in Fig. 13 that, when the combined soil layer changes from very stiff (black dot line) to very soft (green dot line), the dynamic response of the tunnel lining keeps the same primary common peak frequency at about 72 Hz but gets larger amplitude mainly in low frequency band (roughly below 200 Hz). The tunnel vibrates stronger in low frequency band when the combined soil layer is softer.

Figure 14 shows the shows the influence of the soil stiffness on the response at the −4th floor of the building.

It can be seen in Fig. 14 that, in general, with lower soil stiffness, the response at the −4th floor has lower high frequency contents roughly above 100 Hz and higher low frequency contents roughly below 80 Hz.

The influence of soil stiffness on the vibration transfer along the floors is investigated using the indicator amplification scale as mentioned before. Figure 15 shows the results at several frequencies (1/3 octave bands) for example.

It can be seen in Fig. 15 that the vibration transfer along the floors is influenced heavily by the soil stiffness. The influence is nonlinear and frequency-dependent. However, the influence is mainly on the amplitudes rather than on the trends of the amplification scale. At low frequencies, the amplification scale is generally growing along the floors, while at high frequencies, the amplification scale is generally reducing along the floors.

6 Conclusions and future work

In this work, an explicit-integration time-domain, fully coupled 3D dynamic train-track-tunnel-soil-building FE model is developed and validated with in-situ experimental results. Good agreements between the numerical and experimental results have been achieved both in time domain and frequency domain. The vibration transfer from an underground train to a typical multi-story building has been successfully simulated.

The vibration of the multi-story building is investigated through the analysis of the amplification scale along the height of the building and the modal analysis using the FE method. Consistencies between the amplification scale
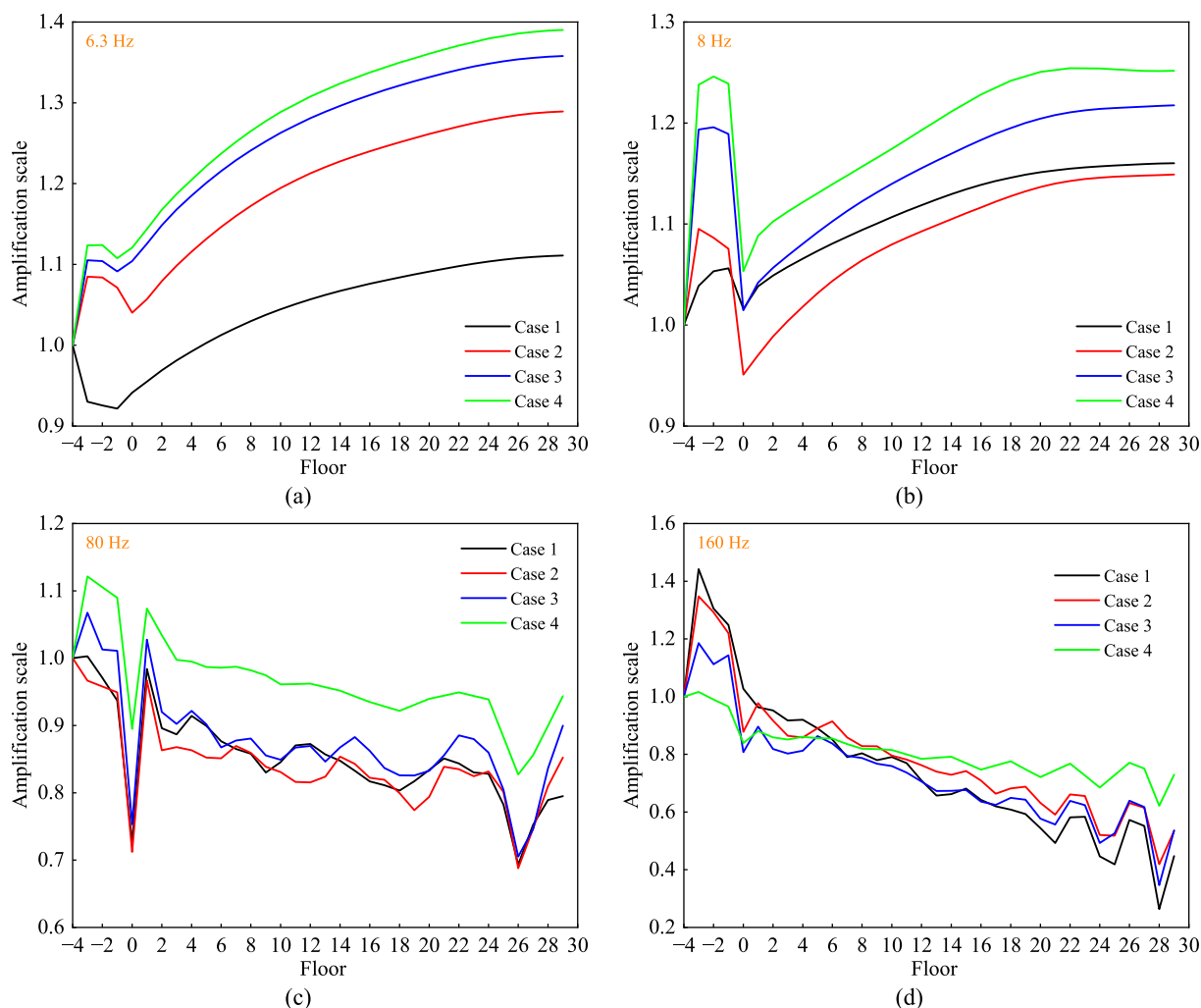
Fig. 15. Influences of soil stiffness on the vibration transfer along the floors. (a) 6.3 Hz, (b) 8 Hz, (c) 80 Hz, and (d) 160 Hz.

along the height of the building and the building resonances can be found. In general, from the foundation to the top floor, the vertical vibration level decreases due to the loss of high frequency contents. The vertical vibration levels in different rooms at a same floor can be different due to the different local stiffness. A larger room has larger vibration level because of its smaller local stiffness while a smaller room has lower vibration level due to its higher local stiffness. The vibration in the building transferred from the underground train is dominant at the frequency determined by the P2 resonance and influenced by the vibration modes of the building.

The influence of the soil stiffness on the vibration transfer is investigated. It is found that the soil stiffness has very limited influence on the dynamic responses of the rail and the track slab. The tunnel wall and the building could have relative higher low frequency vibration (roughly below 80 Hz) when the soil gets softer. The vibration transfer along the floors of the building is influenced heavily by the soil stiffness in terms of the amplitudes of the amplification scale. The influence is nonlinear and frequency-dependent, which needs to be further investigated.

In the future, the developed explicit-integration time-domain 3D dynamic train-track-tunnel-soil-building FE model will be employed to further investigate the vibration transfer from the underground train to the building with more considerations on the nonlinearities in soil properties, structure-soil interactions and track components.

Data availability

The data that support the findings of this study are available from the corresponding author upon reasonable request.

CRediT authorship contribution statement

Li Wang: Conceptualization, Formal analysis, Methodology, Writing – original draft, Writing – review & editing. **Xin Gao:** Data curation, Formal analysis, Methodology, Writing – review & editing. **Caiyou Zhao:** Conceptualization, Data curation, Funding acquisition, Investigation, Methodology, Supervision, Writing – review & editing. **Ping Wang:** Conceptualization, Funding acquisition, Inves-

tigation, Methodology, Project administration, Supervision, Writing – review & editing. **Zili Li:** Conceptualization, Methodology, Resources, Software, Supervision, Writing – review & editing.

Declaration of competing interest

The authors declare that they have no known competing financial interests or personal relationships that could have appeared to influence the work reported in this paper.

References

Cao, Z. L., Guo, T., Zhang, Z. Q., & Li, A. Q. (2018). Measurement and analysis of vibrations in a residential building constructed on an elevated metro depot. *Measurement, 125*, 394–405.

Colaço, A., Barbosa, D., & Costa, P. A. (2022). Hybrid soil-structure interaction approach for the assessment of vibrations in buildings due to railway traffic. *Transportation Geotechnics, 32*, 100691.

Connolly, D. P., Marecki, G. P., Kouroussis, G., Thalassinakis, I., & Woodward, P. K. (2016). The growth of railway ground vibration problems — A review. *Science of Total Environment, 568*, 1276–1282.

Coulier, P., Lombaert, G., & Degrande, G. (2014). The influence of source–receiver interaction on the numerical prediction of railway induced vibrations. *Journal of Sound and Vibration, 333*(12), 2520–2538.

Deutsches Institut für Normung. (1999). DIN4150-2: Structural vibrations - Part 2: Human exposure to vibration in buildings.

He, C., Zhou, S. H., & Guo, P. J. (2020). An efficient three-dimensional method for the prediction of building vibrations from underground railway networks. *Soil Dynamics and Earthquake Engineering, 139*, 106269.

Ibrahim, Y. E., & Nabil, M. (2021). Finite element analysis of multistory structures subjected to train-induced vibrations considering soil-structure interaction. *Case Studies in Construction Materials, 15*, e00592.

International Organization for Standardization. (1997). *ISO 2631-1:1997: Mechanical vibration and shock – Evaluation of human exposure to whole-body vibration – Part 1: General requirements.*

International Organization for Standardization. (2013) *ISO 3095:2013*: Acoustics - Railway applications - Measurement of noise emitted by railbound vehicles.

Ju, S. H. (2007). Finite element analysis of structure-borne vibration from high-speed train. *Soil Dynamics and Earthquake Engineering, 27*(3), 259–273.

Kouroussis, G., Verlinden, O., & Conti, C. (2011). Free field vibrations caused by high-speed lines: Measurement and time domain simulation. *Soil Dynamics and Earthquake Engineering, 31*(4), 692–707.

Li, T., Su, Q., & Kaewunruen, S. (2020). Influences of piles on the ground vibration considering the train-track-soil dynamic interactions. *Computer and Geotechnics, 120*, 103455.

Liang, R. H., Ding, D. Y., Liu, W. F., Sun, F. Q., & Cheng, Y. L. (2023). Experimental study of the source and transmission characteristics of train-induced vibration in the over-track building in a metro depot. *Journal of Vibration and Control, 29*(7–8), 1738–1751.

Liang, R. H., Liu, W. F., Li, W. B., & Wu, Z. Z. (2022). A traffic noise source identification method for buildings adjacent to multiple transport infrastructures based on deep learning. *Building and Environment, 211*, 108764.

Lopes, P., Costa, P. A., Calçada, R., & Cardoso, A. S. (2014a). Influence of soil stiffness on building vibrations due to railway traffic in tunnels: Numerical study. *Computer and Geotechnics, 61*, 277–291.

Lopes, P., Costa, P. A., Ferraz, M., Calçada, R., & Cardoso, A. S. (2014b). Numerical modeling of vibrations induced by railway traffic in tunnels: From the source to the nearby buildings. *Soil Dynamics and Earthquake Engineering, 61–62*, 269–285.

Ma, M., Li, M. H., Qu, X. Y., & Zhang, H. G. (2022). Effect of passing metro trains on uncertainty of vibration source intensity: Monitoring tests. *Measurement, 193*, 110992.

Ma, M., Liu, W.N., Markine, V.L., Liu, W.F., & Sun, X.J. (2011a). Measurement of vibrations induced by road traffic and subway trains in laboratory. In G. De Roeck, G. Degrande, G. Lombaert, & G. Muller (Eds.), *Proceedings of the 8th international conference on structural dynamics, EURODYN 2011.*

Ma, M., Markine, V. L., Liu, W. N., Yuan, Y., & Zhang, F. (2011b). Metro train-induced vibrations on historic buildings in Chengdu, China. *Journal of Zhejiang University- Science A, 12*(10), 782–793.

Ma, M., Xu, L. H., Du, L. L., Wu, Z. Z., & Tan, X. Y. (2021). Prediction of building vibration induced by metro trains running in a curved tunnel. *Journal of Vibration and Control, 27*(5–6), 515–528.

Mendoza, D. L., Connolly, D. P., Romero, A., Kouroussis, G., & Galvín, P. (2020). A transfer function method to predict building vibration and its application to railway defects. *Construction and Building Materials, 232*, 117217.

Ministry of Ecology and Environment of the People's Republic of China (2018). *HJ 453—2018*: Technical guidelines for environmental impact assessment – urban rail transit. China Environment Publishing Group (in Chinese).

Qu, S., Yang, J. J., Zhu, S. Y., Zhai, W. M., & Kouroussis, G. (2021). A hybrid methodology for predicting train-induced vibration on sensitive equipment in far-field buildings. *Transportation Geotechnics, 31*, 100682.

Qu, X. Y., Thompson, D., Ma, M., Li, M. H., & Evangelos, N. (2023). Sources of variability in metro train-induced vibration. *Proceedings of the Institution of Mechanical Engineers, Part F: Journal of Rail and Rapid Transit, 237*(4), 490–499.

Sanayei, M., Maurya, P., & Moore, J. A. (2013). Measurement of building foundation and ground-borne vibrations due to surface trains and subways. *Engineering Structures, 53*, 102–111.

Sanitate, G., & Talbot, J. P. (2023). Foundation vibration and the added-building effect: Experimental evidence from a ground-borne vibration measurement campaign. *Journal of Sound and Vibration, 544*, 117390.

Sheng, X. Z. (2019). A review on modelling ground vibrations generated by underground trains. *International Journal of Rail Transportation, 7*(4), 241–261.

Thompson, D. J., Kouroussis, G., & Ntotsios, E. (2019). Modelling, simulation and evaluation of ground vibration caused by rail vehicles. *Vehicle System Dynamics, 57*(7), 936–983.

Trochides, A. (1991). Ground-borne vibrations in buildings near subways. *Applied Acoustics, 32*(4), 289–296.

Wang, L., Wang, P., Wei, K., Dollevoet, R., & Li, Z. (2022). Ground vibration induced by high speed trains on an embankment with pile-board foundation: Modelling and validation with in situ tests. *Transportation Geotechnics., 34*, 100734.

Wang, S., Xin, T., Wang, P., Yang, Y., Chen, P., Zhao, L., Zhao, S., & Luo, Y. (2022). Numerical study on high-frequency effect of rail corrugation on subway-induced environmental vibrations. *Environmental Science and Pollution Research, 29*(53), 80657–80668.

State Environmental Protection Administration. (1988). *GB 10070—88: Standard of environmental vibration in urban area.* Beijing: Standards Press of China. (in Chinese).

Wei, D., Shi, W.X., Han, R.L., & Zhang, S.L. (2011). Measurement and research on subway induced vibration in tunnels and building nearby in Shanghai. In *2011 International Conference on Multimedia Technology* (pp. 1602–1605). Hangzhou, China.

Xia, H., Chen, J. G., Wei, P. B., & Xia, C. Y. (2009). Experimental investigation of railway train-induced vibrations of surrounding ground and a nearby multi-story building. *Earthquake Engineering and Engineering Vibration, 8*(1), 137–148.

Xu, Q. Y., Ou, X., Au, F. T. K., Lou, P., & Xiao, Z. C. (2016). Effects of track irregularities on environmental vibration caused by underground railway. *European Journal of Mechanics – A, 59*, 280–293.

Yang, J. J., Zhu, S. Y., Zhai, W. M., Kouroussis, G., Wang, Y., Wang, K. Y., Lan, K., & Xu, F. Z. (2019). Prediction and mitigation of train-induced vibrations of large-scale building constructed on subway tunnel. *Science of Total Environment, 668*, 485–499.

Yang, Y. B., & Hung, H. H. (2008). Soil vibrations caused by underground moving trains. *Journal of Geotechnical and Geoenvironmental Engineering, 134*(11), 1633–1644.

Zou, C., Moore, J. A., Sanayei, M., Wang, Y., & Tao, Z. (2021). Efficient impedance model for the estimation of train-induced vibrations in over-track buildings. *Journal of Vibration and Control, 27*(7–8), 924–942.

Zou, C., Wang, Y. M., Wang, P., & Guo, J. X. (2015). Measurement of ground and nearby building vibration and noise induced by trains in a metro depot. *Science of Total Environment, 536*, 761–773.